EUROPEAN ORGANIZATION FOR NUCLEAR RESEARCH

CERN-EP/2000-120
11 September 2000

Study of Z Boson Pair Production in e^+e^- Interactions at $\sqrt{s} = 192 - 202$ GeV

The L3 Collaboration

Abstract

The cross section for the production of Z boson pairs is measured using the data collected by the L3 detector at LEP in 1999 in e^+e^- collisions at centre-of-mass energies ranging from 192 GeV up to 202 GeV. Events in all the visible final states are selected, measuring the cross section of this process. The special case of final states containing b quarks is also investigated. All results are in agreement with the Standard Model predictions.

Submitted to *Phys. Lett. B*

1 Introduction

The increase of the LEP centre-of-mass energy, $\sqrt{s}$, beyond the Z pole has extended the range of the accessible physics processes to include a sizable fraction of four-fermion events. An important part of the four-fermion final states emerges from the pair production of W or Z gauge bosons.

The study of Z boson pair-production is of interest as it offers a further test of the Standard Model of the electroweak interactions [1] in the neutral gauge boson sector. Moreover, this process constitutes a background in the search of the Standard Model Higgs boson. In addition, Z-pair events allow the investigation of possible triple neutral gauge boson couplings, ZZZ and ZZγ [2,3], forbidden at tree level in the Standard Model. These events can also test new theories beyond the Standard Model such as Supersymmetry [3,4] or extra space dimensions [5].

At the lowest order, Z pair-production proceeds via two t-channel Feynman diagrams with an internal electron leg. Considering the Z decays into fermions, this process is conventionally denoted as NC02, from the acronym of the neutral-current production mechanism of the four-fermions and the number of diagrams. A wider definition is used in this letter, encompassing the regions of the full four-fermion phase space compatible with the pair-production of Z bosons. Results in the NC02 framework are also given.

The experimental investigation of the Z pair-production is made difficult by its rather low cross section, compared with competing two- and four-fermion processes, that constitute large and sometimes irreducible backgrounds. This process was observed at threshold by the L3 collaboration at $\sqrt{s} = 183$ GeV [6] and studied later with a higher statistical sample at $\sqrt{s} = 189$ GeV [7]. Results from the other LEP collaborations were also reported [8]. This letter describes the extension of the L3 analyses to centre-of-mass energies between 192 GeV and 202 GeV. The measurement of the cross section is presented together with other results that include lower centre-of-mass energies. The measurement of the cross section for the particular case of Z pair-production and decay into at least a b quark pair is also discussed.

2 Data and Monte Carlo Samples

The data under investigation were collected in 1999 by the L3 detector [9] at four different centre-of-mass energies, 191.6 GeV, 195.5 GeV, 199.5 GeV and 201.7 GeV with corresponding integrated luminosities of $29.7\,\mathrm{pb}^{-1}$, $83.7\,\mathrm{pb}^{-1}$, $82.8\,\mathrm{pb}^{-1}$ and $37.0\,\mathrm{pb}^{-1}$. These energies are denoted as 192, 196, 200 and 202 hereafter.

The EXCALIBUR [10] Monte Carlo is used to generate events belonging to both the signal and the background neutral-current four-fermion processes. Background from fermion-pair production is described making use of PYTHIA [11] and KK2f [12] ($\mathrm{e^+e^-} \to \mathrm{q\bar{q}}(\gamma)$), KORALZ [13] and KK2f ($\mathrm{e^+e^-} \to \mu^+\mu^-(\gamma)$ and $\mathrm{e^+e^-} \to \tau^+\tau^-(\gamma)$) and BHWIDE [14] ($\mathrm{e^+e^-} \to \mathrm{e^+e^-}(\gamma)$). Background from charged-current four-fermion processes is generated with EXCALIBUR for $\mathrm{e}\nu_\mathrm{e}\mathrm{q\bar{q}'}$ and $\ell^+\nu_\ell\ell^-\bar{\nu}_\ell$ with $\ell = \mathrm{e}, \mu, \tau$ and KORALW [15] for W pair-production and decay in the final states not covered by the simulations listed above. Contributions from multi-peripheral processes are modelled by PHOJET [16] ($\mathrm{e^+e^-} \to \mathrm{e^+e^-q\bar{q}}$) and DIAG36 [17] ($\mathrm{e^+e^-} \to \mathrm{e^+e^-}\ell^+\ell^-$), in the quark and lepton low invariant mass region not included in the samples generated with EXCALIBUR.

The L3 detector response is simulated using the GEANT program [18], which takes into account the effects of energy loss, multiple scattering and showering in the detector. Time dependent detector inefficiencies, as monitored during the data taking period, are reproduced in these simulations.

The Z pair-production signal is defined as the subset of the full four-fermion phase space satisfying the following requirements [6, 7]. First, the invariant mass of both fermion pairs must be between 70 GeV and 105 GeV. In the case in which fermion pairs can originate from a charged-current process ($\mathrm{u\bar{d}d\bar{u}}$, $\mathrm{c\bar{s}s\bar{c}}$ and $\nu_\ell \ell^+ \bar{\nu}_\ell \ell^-$, with $\ell = \mathrm{e}, \mu, \tau$), the masses of the fermion pairs which can also emerge from W decays are required to be either below 75 GeV or above 85 GeV. Finally, events with electrons in the final state are rejected if for any electron $|\cos\theta_\mathrm{e}| > 0.95$, where θ_e is the electron polar angle.

The expected cross sections for the different final states are computed imposing the requirements described above on a sample of events generated with EXCALIBUR, and found to be 0.79 pb, 0.92 pb, 1.00 pb and 1.03 pb at the four centre-of-mass energies, in increasing order. In this calculation $\alpha_s = 0.119$ [19] is included for the QCD vertex corrections. An uncertainty of $\pm 2\%$ is assigned to these predictions, reflecting the differences between them and those obtained with the GRC4F [20] Monte Carlo generator as well as the expected accuracy of the treatment of initial state radiation.

The relative populations of the different channels, as obtained from their corresponding cross sections, differ slightly from those of the NC02 framework, derived from the Z branching ratios [19].

The cross section for final states with at least one b quark pair is significantly smaller than the total cross section and all centre-of-mass energies are hence combined. The corresponding predicted cross section is 0.27 pb with an uncertainty of $\pm 2\%$.

3 Event Selection

All the visible final states of the Z-pair decay are investigated with criteria similar to those used at $\sqrt{s} = 189$ GeV [7], and modified to follow the evolution of the signal topology, which manifests a larger boost of the Z bosons with the higher $\sqrt{s}$. All selections are based on the identification of two fermion pairs, each with a mass close to the Z boson mass.

Electrons are recognised from energy depositions in the electromagnetic calorimeter whose shower shape is compatible with that initiated by an electron or a photon. According to the selection channel, a track as reconstructed in the central tracker may be required to be associated to this cluster.

Muons are reconstructed either from tracks in the muon spectrometer pointing to the interaction vertex and in time with the event, or via only energy depositions in the calorimeters consistent with a minimum ionising particle (MIP) which have a matching track in the central tracker.

Tau leptons are identified from their decay into electrons or muons or as low-multiplicity jets with one or three associated tracks. A total unit charge is required.

Quarks manifest themselves with a high multiplicity of calorimetric clusters and charged tracks. These are grouped into the required number of jets by means of the DURHAM algorithm [21].

The hermeticity of the detector allows to reconstruct the four-momentum of Z bosons decaying into neutrinos by means of the event missing energy and the momentum imbalance.

The selection criteria specific for each final state are discussed below, first for the channels containing hadrons, then for the purely leptonic ones.

3.1 The $q\bar{q}\ell^+\ell^-$ Channel

For each of the final states $q\bar{q}e^+e^-$, $q\bar{q}\mu^+\mu^-$ and $q\bar{q}\tau^+\tau^-$, a dedicated selection is performed. A pair of leptons should be present in high multiplicity events with visible energy and effective centre-of-mass energy respectively in excess of $0.5\sqrt{s}$ and $0.6\sqrt{s}$. The effective centre-of-mass energy is the energy at which the e^+e^- interaction takes place after the possible emission of initial state radiation photons. It is reconstructed taking into account both photons observed in the detector and those collinear with the beam axis [22]. For the $q\bar{q}e^+e^-$ selection, at least one electron is required to have a matched track. No more than one MIP is allowed in the $q\bar{q}\mu^+\mu^-$ selection.

The $q\bar{q}\tau^+\tau^-$ selection relies on both a particle-based and a jet-based approach. The former is aimed to identify a pair of taus in the events while in the latter the event is constrained into four-jets. Two of the jets must have less than four tracks and are considered as the tau candidates. At least one of them has also to coincide with an identified tau. The radiative $q\bar{q}(\gamma)$ background is further suppressed by rejecting events containing a photon of energy larger than 40 GeV.

The topology of the pair-production of Z bosons is enforced by requiring the lepton pair and the jet pair to have an opening angle of at least 110° for the electron and muon channels and 120° for the tau channel. Moreover, the invariant mass of the jet-jet and the lepton-lepton systems after performing a kinematic fit, which imposes energy and momentum conservation, must be between 70 GeV and 120 GeV, as depicted in Figure 1a for the lepton case.

The contribution from semileptonic decays of W pairs is reduced by requiring the transverse missing momentum to be lower than $0.2\sqrt{s}$ and the visible energy in the electron and muon channels to be at least $0.85\sqrt{s}$, while it has to be between $0.6\sqrt{s}$ and $0.9\sqrt{s}$ for the tau selections.

To reject the residual background from W pair-production and hadronic events with gluon radiation, the events are subject to the DURHAM algorithm requiring y_{34} to be greater than 0.001 for the electron and muon channels and 0.0025 for the tau channel. y_{34} is the DURHAM resolution parameter for which events change from a three-jet into a four-jet topology.

The kinematic fit is repeated on events that pass at least one of the three selections described above, with the additional constraint of equal invariant masses for the jet-jet and lepton-lepton systems. The distribution of this invariant mass, M_{5C}, is shown in Figure 1b. Table 1 summarises the efficiencies achieved by the different selections. Tables 2 and 3 present respectively the total yield of the selection and its breakdown into the different centre-of-mass energies. Efficiencies are calculated from Monte Carlo events retained by at least one of the selections described above.

	Selection			
Final State	$e^+e^-q\bar{q}$	$\mu^+\mu^-q\bar{q}$	$\tau^+\tau^-q\bar{q}$	Total
$e^+e^-q\bar{q}$	77.2%	–	2.6%	79.5%
$\mu^+\mu^-q\bar{q}$	–	53.7%	6.2%	59.2%
$\tau^+\tau^-q\bar{q}$	0.6%	0.2%	28.2%	28.7%

Table 1: Efficiency of the $q\bar{q}\ell^+\ell^-$ selections and of their combination.

Selection	Data	Signal MC	Background MC	Efficiency
$\mathrm{q\bar{q}}\ell^+\ell^-$	31	18.8 ± 0.2	4.9 ± 0.4	56.5%
$\mathrm{q\bar{q}}\nu\bar{\nu}$	89	33.9 ± 0.2	57.7 ± 0.3	55.4%
$\mathrm{q\bar{q}q'\bar{q}'}$	530	69.3 ± 0.3	445.1 ± 3.3	65.0%
$\ell^+\ell^-\nu\bar{\nu}$	3	2.5 ± 0.1	3.2 ± 0.1	40.5%
$\ell^+\ell^-\ell'^+\ell'^-$	3	1.3 ± 0.0	1.0 ± 0.3	39.4%

Table 2: Data, signal and background Monte Carlo events selected by each analysis and their efficiency. The $\mathrm{q\bar{q}}\nu\bar{\nu}$ and $\mathrm{q\bar{q}q'\bar{q}'}$ entries are reported for selection requirements of 0.5 and 0.2 on the neural network outputs, respectively. The $\ell^+\ell^-\nu\bar{\nu}$ entries refer only to electrons and muons. The uncertainties shown are from Monte Carlo statistics. Efficiencies are averaged over the four centre-of-mass energies and do not present any significative dependence on $\sqrt{s}$.

3.2 The $\mathrm{q\bar{q}}\nu\bar{\nu}$ Channel

The selection of the $\mathrm{q\bar{q}}\nu\bar{\nu}$ channel proceeds from high multiplicity events with an invariant mass in excess of 50 GeV. These criteria deplete the total data sample of purely leptonic two-fermion final states and products of two-photon interactions. Hadronic events from $\mathrm{q\bar{q}}(\gamma)$ and W pair-production are then reduced by requiring the invariant mass to be less than 130 GeV and the mass recoiling against the hadronic system to exceed 50 GeV. Semileptonic decays of W pairs are suppressed by rejecting events with electrons or muons with energies above 20 GeV. The missing energy signature of a Z boson decaying into two neutrinos is further exploited by requiring the transverse momentum to be above 5 GeV, the energy deposition in the forward calorimeters to be below 10 GeV and the missing momentum vector to point at least 16° away from the beam axis. Moreover, the energy in a 25° azimuthal sector around the missing energy direction, E_{25}, must not exceed 30 GeV.

The selection requirements described above select 407 events in the full data sample. The Monte Carlo expectations are 45 events for the signal and 339 for the background, mainly accounted for by charged-current four-fermion processes.

An artificial neural network is then designed to further discriminate Z pair events from background. It is based on event shape variables that differentiate the two-jet from the three-jet topology, on the sum of invariant and missing masses, on the masses of the two jets into which the event can be forced, the total missing momentum and E_{25}. A constrained fit is applied to the hadronic system in the hypothesis that the missing energy and momenta are due to a Z boson. The resulting mass M_{fit}, presented in Figure 1c, is also used in the neural network. The output NN_{Out} of the neural network is presented in Figure 1d. The efficiency and the results of this selection are summarised in Table 2 and detailed in Table 3 for the different centre-of-mass energies for a benchmark cut of 0.5 on NN_{Out}.

3.3 The $\mathrm{q\bar{q}q'\bar{q}'}$ Channel

The $\mathrm{q\bar{q}q'\bar{q}'}$ channel is investigated by first selecting high-multiplicity events with a visible energy between $0.6\sqrt{s}$ and $1.4\sqrt{s}$, parallel and perpendicular imbalances below $0.3\sqrt{s}$ and no identified electron, muon or photon with energy above 65 GeV. The events are forced to four jets and then subjected to a constrained fit which rescales the jets to balance momentum while imposing energy conservation, greatly reducing the dependence on the calorimeter energy scale.

Such hadronic events are copiously produced in QCD processes and W-pair production.

$\sqrt{s}$ (GeV)	N_D	N_S	N_B	N_D	N_S	N_B
	$q\bar{q}\ell^+\ell^-$			$q\bar{q}\nu\bar{\nu}$		
192	2	2.0 ± 0.1	0.4 ± 0.1	3	3.5 ± 0.1	4.5 ± 0.1
196	13	6.7 ± 0.1	2.0 ± 0.3	35	11.9 ± 0.1	18.6 ± 0.1
200	13	6.9 ± 0.1	1.8 ± 0.3	35	12.6 ± 0.1	23.1 ± 0.1
202	3	3.2 ± 0.1	0.7 ± 0.1	16	5.9 ± 0.1	11.5 ± 0.1
	$q\bar{q}q'\bar{q}'$			$\ell^+\ell^-\nu\bar{\nu}$		
192	46	7.0 ± 0.1	49.0 ± 1.7	0	0.28 ± 0.02	0.44 ± 0.02
196	178	23.5 ± 0.2	155.1 ± 1.9	1	0.82 ± 0.06	0.88 ± 0.04
200	199	26.6 ± 0.2	162.8 ± 1.7	2	0.92 ± 0.04	1.38 ± 0.12
202	107	12.2 ± 0.1	78.2 ± 1.2	0	0.45 ± 0.03	0.49 ± 0.03
	$\ell^+\ell^-\ell'^+\ell'^-$			$e^+e^- \rightarrow ZZ$		
192	0	0.16 ± 0.01	0.24 ± 0.04	51	12.9 ± 0.1	54.6 ± 1.7
196	1	0.50 ± 0.02	0.42 ± 0.15	228	43.4 ± 0.2	177.0 ± 1.9
200	2	0.44 ± 0.02	0.30 ± 0.09	251	47.4 ± 0.2	189.4 ± 1.7
202	0	0.21 ± 0.01	0.09 ± 0.19	126	22.0 ± 0.2	91.0 ± 1.2

Table 3: Number of data (N_D), signal (N_S) and background (N_B) Monte Carlo events selected at the different centre-of-mass energies in the separate final states and their sum. The $q\bar{q}\nu\bar{\nu}$ and $q\bar{q}q'\bar{q}'$ entries are reported for selection requirements on the neural network outputs of 0.5 and 0.2, respectively. Monte Carlo statistical uncertainties are given on the signal and background expectations.

Two artificial neural networks are sequentially constructed to isolate the Z pair signal and reject these two backgrounds. The first neural network [23] helps in selecting the signal from the QCD background. After a cut at 0.65 on the output of this neural network, displayed in Figure 2a, the content in W and Z pair production events is enhanced.

A second neural network is then built to distinguish Z pairs from W pairs. It relies on the reconstructed di-jet mass, the maximum and minimum jet energy, the average number of charged tracks per jet and the di-jet mass difference.

Almost 40% of the events generated in the $q\bar{q}q'\bar{q}'$ channel and satisfying the signal definition contain at least a b quark pair, while the b-content in W pair events is negligible. A b-tag discriminant [24], is then added to the network to further discriminate Z pair from W pair events.

Figure 2b displays the output of this network after the W pair enriched region below 0.2 is discarded. Events compatible with Z pair-production preferentially populate the region between 0.6 and 0.8 if their content in b quarks is low and lie above otherwise. The performances of this analysis are summarised in Tables 2 and 3.

These results are confirmed by a simpler cut-based analysis that relies on the signature of the different boost of Z and W pairs as retained in the two di-jet opening angles, the di-jet mass difference and the di-jet mean mass. Another study mainly aimed at the rejection of the QCD background and the simultaneous selection of four-jet W and Z pair events also yields compatible results. Both these analyses are affected by a lower purity which follows from the absence of a b-tag.

3.4 The $\ell^+\ell^-\nu\bar{\nu}$ Channel

A pair of identified electrons or muons constitutes the core of the $\ell^+\ell^-\nu\bar{\nu}$ selection. Tracks are not required for the electron identification and MIPs are not considered as muon candidates. The lepton pair must be consistent with a Z boson, with an invariant mass, $M_{\ell\ell}$, between 80 GeV and 100 GeV. The recoil mass, M_{rec}, is required to lie in the same interval to enforce the signature of the second Z decaying into two neutrinos.

Fermion-pair events are rejected by requiring the lepton pair to be acoplanar and to have a visible energy compatible with the signal hypothesis. Moreover, the missing momentum vector must point away from the beam line.

The background from other resonant and non-resonant four-fermion processes is reduced by performing a kinematic fit which imposes the Z mass to the visible pair of leptons. The recoil mass M_{rec}^{fit} is recalculated and required to be compatible with the Z mass.

The distribution of the sum of $M_{\ell\ell}$ and M_{rec} is expected to peak around twice the Z mass for signal events, and is presented in Figure 2c. The efficiency of the selection is reported in Table 2, which also lists the total number of selected and expected events, detailed in Table 3 for the different centre-of-mass energies. No contribution from the $\tau^+\tau^-\nu\bar{\nu}$ signal is expected after this selection. The dominant background arises from charged-current four-fermion processes.

3.5 The $\ell^+\ell^-\ell'^+\ell'^-$ Channel

To achieve a high efficiency, the selection of the $\ell^+\ell^-\ell'^+\ell'^-$ channel starts from four or more loosely identified leptons in low-multiplicity events and concentrates on the kinematic properties of just a pair of them. Electrons with or without a matched track, muons and taus are accepted in the first stage, provided their energy exceeds 3 GeV. If more than four leptons are present, the four most compatible with energy and momentum conservation are selected.

The event must contain at least an electron or a muon pair. To form such pairs at least one electron should have a matched track and no MIPs are considered as muons. In the case of multiple choices, the pair with the invariant mass $M_{\ell\ell}$ closest to the Z mass is studied. Both $M_{\ell\ell}$ and the recoil mass M_{rec} to this selected lepton pair are required to be in the range between 70 GeV and 105 GeV.

Selection criteria on the energy of the most energetic electromagnetic cluster of the event and the acoplanarity and acollinearity of the lepton pair reject the residual Bhabha and radiative fermion pair-production backgrounds.

The data and Monte Carlo distributions for the sum of $M_{\ell\ell}$ and M_{rec}, the most discriminating variable between signal and background, are displayed in Figure 2d. The yield of the selection for the total sample, and the separate energies are respectively given in Tables 2 and 3. The background is mainly constituted by non-resonant neutral-current four-fermion events.

4 Results

4.1 Measurement of the ZZ Cross Section

The distributions of the variables presented in Figures 1b, 1d, 2b, 2c and 2d are separated into each centre-of-mass energy and are then fit to determine the cross section of the individual channels.

A probability density function is built from the observed number of events in each of the bins of the distribution as a function of the signal cross section, fixing the background expectations. A flat positive distribution for its value is assumed. If a zero value of the cross section is contained in a ±34% confidence interval around the maximum of the probability density function, then a 95% confidence level upper limit is calculated. This maximum is otherwise quoted as the measurement, adopting this interval as the corresponding statistical uncertainty.

Table 4 lists the results of all these fits together with the Standard Model predictions. Assuming these predictions as the relative weights of the different channels, the ZZ cross section for each centre-of-mass energy can be calculated from a simultaneous fit to the five channels. The results of this fit are also presented in Table 4. All the measured cross sections agree with the Standard Model predictions. In the calculation of the cross section, the effect of the cross talk between the separate channels is found to be negligible.

$\sqrt{s}$	σ^{fit} (pb)	σ^{th} (pb)	σ^{fit} (pb)	σ^{th} (pb)	σ^{fit} (pb)	σ^{th} (pb)
(GeV)	$\mathrm{q\bar{q}}\ell^+\ell^-$		$\mathrm{q\bar{q}}\nu\bar{\nu}$		$\mathrm{q\bar{q}q'\bar{q}'}$	
192	< 0.36	0.12	< 0.28	0.22	< 0.73	0.38
196	0.20 ± 0.07	0.14	0.25 ± 0.11	0.25	0.63 ± 0.20	0.44
200	0.22 ± 0.08	0.15	0.25 ± 0.12	0.28	0.60 ± 0.20	0.48
202	< 0.32	0.15	0.16 ± 0.15	0.29	0.84 ± 0.33	0.49
	$\ell^+\ell^-\nu\bar{\nu}$		$\ell^+\ell^-\ell'^+\ell'^-$		$\mathrm{e^+e^-} \rightarrow \mathrm{ZZ}$	
192	< 0.26	0.03	< 0.11	0.01	0.29 ± 0.22	0.79
196	< 0.19	0.04	< 0.11	0.01	1.17 ± 0.24	0.92
200	< 0.24	0.04	0.06 ± 0.04	0.01	1.25 ± 0.25	1.00
202	< 0.26	0.04	< 0.13	0.01	0.93 ± 0.38	1.03

Table 4: Results, σ^{fit}, of the individual and global cross section fits for the different centre-of-mass energies. The corresponding theory predictions, σ^{th}, are also given. Limits are at 95% confidence level.

Figure 3a presents the distribution of the reconstructed mass, M, for all the selected events, including those collected at lower centre-of-mass energies [6, 7]. A cut on the $\mathrm{q\bar{q}}\nu\bar{\nu}$ and $\mathrm{q\bar{q}q'\bar{q}'}$ neural network outputs at 0.8 and 0.85 is applied, respectively. For the $\mathrm{q\bar{q}}\ell^+\ell^-$ and the $\mathrm{q\bar{q}}\nu\bar{\nu}$ channels, M corresponds to M_{5C} and M_{fit}, respectively. The average of the two di-jet masses is considered for the $\mathrm{q\bar{q}q'\bar{q}'}$ channel while for both the $\ell^+\ell^-\nu\bar{\nu}$ and $\ell^+\ell^-\ell'^+\ell'^-$ channels the average of $M_{\ell\ell}$ and M_{rec} is used. A fit to the distribution of M is performed in terms of the ratio R_{ZZ} between the observed events and the predictions from Z pair-production and yields:

$$R_{\mathrm{ZZ}} = 0.94 \pm 0.14 \pm 0.06,$$

in agreement with the Standard Model. The first uncertainty is statistical and the second systematic, discussed in References 6 and 7 and below. The cosine of the observed production polar angle θ is presented in Figure 3b for the same selected events.

4.2 Study of Systematic Uncertainties

Systematic uncertainties on the $\mathrm{e^+e^-} \rightarrow \mathrm{ZZ}$ cross section can be divided into sources correlated and uncorrelated among the channels. Their effects are estimated using the full 1999 data sample, and then propagated to the measurements performed at the different centre-of-mass energies.

The main sources of correlated systematic uncertainty are the background cross sections and the energy scale of the detector. As they modify the shapes of the fit distributions, their effect is evaluated performing a new fit to calculate the cross section once their values are modified as listed in Table 5. Possible non-linearity effects for the energy scale are investigated. The effect of the uncertainty of the LEP beam energy is negligible.

An uncertainty of 2% is attributed to the measured cross section to take into account the difference of the assumed relative weights of the different channels, given by the EXCALIBUR calculation, with respect to those obtained with GRC4F, and to parametrise other uncertainties related to their calculation.

Some sources of systematic uncertainty are uncorrelated among the channels but modify the shape of the output of the final neural network of the $\mathrm{q\bar{q}q'\bar{q}'}$ selection. These are the jet resolution, the charged track multiplicity and the b-tag, and their effect is presented in Table 5. The jet resolution includes a variation of $\pm 2^{\circ}$ on the jet direction and a smearing of y_{34}. A variation of the b-tag discriminant of $\pm 2\%$ models possible systematic effects and includes uncertainties in the Monte Carlo description of b-hadron jets.

Systematic Source	Variation	$\delta\sigma_{\mathrm{ZZ}}$ (%)	$\delta\sigma_{\mathrm{ZZ\to b\bar{b}X}}$ (%)
Correlated sources			
WW cross section	2%	2.4	2.6
Four-jet rate	5%	2.1	3.0
Weν cross section	10%	1.3	< 0.1
Four-fermion cross section	5%	0.3	2.6
Energy scale	2%	3.6	3.9
Lep energy	40 MeV	< 0.1	< 0.1
Theory predictions	2%	2.0	2.0
Uncorrelated sources			
Jet resolution ($\mathrm{q\bar{q}q'\bar{q}'}$)	see text	0.3	0.4
Charge multiplicity ($\mathrm{q\bar{q}q'\bar{q}'}$)	1%	2.0	2.4
B-tag ($\mathrm{q\bar{q}q'\bar{q}'}$)	2%	1.6	7.5
Monte Carlo statistics	see text	3.9	3.3
Simulation/Lepton Id	see text	2.5	1.4
Total		7.5	10.8

Table 5: Systematic uncertainties on σ_{ZZ} and $\sigma_{\mathrm{ZZ\to b\bar{b}X}}$. The total systematic uncertainty is the sum in quadrature of the different contributions.

Three additional sources of systematic uncertainty, uncorrelated among the channels, are considered: the Monte Carlo statistics of the signal and the background and the agreement between data and Monte Carlo. The latter comprises normalisation differences as derived from the comparison of data and Monte Carlo samples five to twenty times larger than the final ones, obtained by relaxing some selection criteria. It also includes differences in the shape of the distribution of the lepton identification variables around the adopted selection requirements. All these uncertainties, listed in Table 6, do not affect the shape of the discriminating distributions

	$q\bar{q}\ell^+\ell^-$	$q\bar{q}\nu\bar{\nu}$	$q\bar{q}q'\bar{q}'$	$\ell^+\ell^-\nu\bar{\nu}$	$\ell^+\ell^-\ell'^+\ell'^-$
Signal MC statistics (σ_{ZZ})	1.1%	0.4%	0.4%	3.2%	2.3%
Background MC statistics (σ_{ZZ})	8.1%	0.3%	0.7%	4.1%	24.8%
Signal MC statistics ($\sigma_{ZZ\to b\bar{b}X}$)	1.5%	1.3%	0.7%	–	–
Background MC statistics ($\sigma_{ZZ\to b\bar{b}X}$)	8.1%	0.6%	1.3%	–	–
Simulation/Lepton Id	1.3%	1.9%	1.2%	4.7%	11.3%

Table 6: Sources of uncorrelated systematic uncertainties on σ_{ZZ} and $\sigma_{ZZ\to b\bar{b}X}$.

and their effect on the total cross section propagates as summarised in Table 5. The total systematic uncertainty is the sum in quadrature of all these contributions. The measured cross sections then read:

$$\begin{aligned}
\sigma_{ZZ}(192\text{ GeV}) &= 0.29 \pm 0.22\,(\text{stat.}) \pm 0.02\,(\text{syst.})\text{ pb} \quad (\text{SM}: 0.79 \pm 0.02\,\text{pb}),\\
\sigma_{ZZ}(196\text{ GeV}) &= 1.17 \pm 0.24\,(\text{stat.}) \pm 0.09\,(\text{syst.})\text{ pb} \quad (\text{SM}: 0.92 \pm 0.02\,\text{pb}),\\
\sigma_{ZZ}(200\text{ GeV}) &= 1.25 \pm 0.25\,(\text{stat.}) \pm 0.09\,(\text{syst.})\text{ pb} \quad (\text{SM}: 1.00 \pm 0.02\,\text{pb}),\\
\sigma_{ZZ}(202\text{ GeV}) &= 0.93 \pm 0.38\,(\text{stat.}) \pm 0.07\,(\text{syst.})\text{ pb} \quad (\text{SM}: 1.03 \pm 0.02\,\text{pb}).
\end{aligned}$$

The values in parentheses recall the Standard Model expectations.

A new fit is performed in terms of the NC02 framework and the corresponding cross sections are derived as:

$$\begin{aligned}
\sigma_{ZZ}^{NC02}(192\text{ GeV}) &= 0.29 \pm 0.22\,(\text{stat.}) \pm 0.02\,(\text{syst.})\text{ pb} \quad (\text{SM}: 0.77 \pm 0.02\,\text{pb}),\\
\sigma_{ZZ}^{NC02}(196\text{ GeV}) &= 1.18 \pm 0.24\,(\text{stat.}) \pm 0.09\,(\text{syst.})\text{ pb} \quad (\text{SM}: 0.90 \pm 0.02\,\text{pb}),\\
\sigma_{ZZ}^{NC02}(200\text{ GeV}) &= 1.25 \pm 0.25\,(\text{stat.}) \pm 0.09\,(\text{syst.})\text{ pb} \quad (\text{SM}: 0.98 \pm 0.02\,\text{pb}),\\
\sigma_{ZZ}^{NC02}(202\text{ GeV}) &= 0.95 \pm 0.38\,(\text{stat.}) \pm 0.07\,(\text{syst.})\text{ pb} \quad (\text{SM}: 1.01 \pm 0.02\,\text{pb}).
\end{aligned}$$

The Standard Model expectations given in parentheses are calculated with the ZZTO [25] program and are assigned a $\pm 2\%$ uncertainty [25]. The YFSZZ [26] package yields compatible estimations. As the relative weights of the different final states are set according to the Z boson branching fractions into fermions, the systematic uncertainty no longer includes the $\pm 2\%$ due to their predictions. On the other hand, a $\pm 2\%$ uncertainty is assigned to account for possible effects due to the extrapolation to the NC02 framework of the efficiencies and background estimations from the Monte Carlo simulations described above.

4.3 b Quark Content in ZZ Events

Z pair-production with at least a Z decaying into a b quark pair constitutes an interesting test bench of the detector capabilities to observe the minimal or a supersymmetric Higgs boson. These would in fact be seen as events with heavy particles decaying into a b quark pair, recoiling against a Z boson. Moreover, for the Higgs mass ranges under current investigation at LEP, the cross sections of these processes are similar.

The $q\bar{q}q'\bar{q}'$ final state analysis presents a high sensitivity to final states containing b quarks, as shown in Figure 2b for the $b\bar{b}q\bar{q}$ response of the neural network used to select the $q\bar{q}q'\bar{q}'$ final states.

The $q\bar{q}\nu\bar{\nu}$ and $q\bar{q}\ell^+\ell^-$ selections, as summarised by the distributions of M_{5C} for $q\bar{q}\ell^+\ell^-$ and the neural network output for $q\bar{q}\nu\bar{\nu}$, are complemented with the same b-tag variable as the $q\bar{q}q'\bar{q}'$ selection. Its value is recorded for selected data and Monte Carlo events for each of the two hadronic jets. A single discriminant is then built for each channel from its two b-tag variables and the selection one. First the variables are mapped to achieve uniform distributions for the background. Then the product of their observed values is calculated event by event. Finally the confidence level is calculated for the product of three uniformly distributed quantities to be less than the observed product. This confidence level is expected to be low for signal and flat for background. The final discriminant is the negative logarithm of this confidence level and is presented in Figure 4.

The cross section calculation for the individual channels is performed as for the inclusive modes, considering the distributions in Figures 2b and 4, and yields the results listed in Table 7. The combined result for $\sigma_{ZZ\rightarrow b\bar{b}X}$ is:

$$\sigma_{ZZ\rightarrow b\bar{b}X}(192-202\ \mathrm{GeV}) = 0.31 \pm 0.09\,(\mathrm{stat.})\ \pm 0.03\,(\mathrm{syst.})\,\mathrm{pb},$$

in agreement with the Standard Model expectation of 0.27 ± 0.01 pb. In all fits, the contribution from other Z pair final states are fixed to their Standard Model expectations. The systematic uncertainties are evaluated in the same way as for the total cross section, and are presented in Tables 5 and 6.

	$b\bar{b}\ell^+\ell^-$	$b\bar{b}\nu\bar{\nu}$	$q\bar{q}b\bar{b}$
Measured cross section (pb)	0.07 ± 0.04	< 0.08	0.26 ± 0.07
Expected cross section (pb)	0.031	0.057	0.178

Table 7: Results of the individual ZZ$\rightarrow$ $b\bar{b}$X cross section fits. The limit is at 95% confidence level.

Figure 5 displays the measured total and $b\bar{b}$X cross sections and their expected evolution with $\sqrt{s}$, including data at lower centre-of-mass energies [6, 7] and the theory uncertainties discussed above.

Acknowledgements

We thank the CERN accelerator divisions for the continuous and successful upgrade of the LEP machine and its excellent performance. We acknowledge the contributions of the engineers and technicians who have participated in the construction and maintenance of this experiment.

References

[1] S.L. Glashow, Nucl. Phys. **22** (1961) 579; A. Salam, in Elementary Particle Theory, ed. N. Svartholm, (Almqvist and Wiksell, Stockholm, 1968), p. 367; S. Weinberg, Phys. Rev. Lett. **19** (1967) 1264; M. Veltman, Nucl. Phys. **B 7** (1968) 637; G.M. 't Hooft, Nucl. Phys. **B 35** (1971) 167; G.M. 't Hooft and M. Veltman, Nucl. Phys. **B 44** (1972) 189; G.M. 't Hooft and M. Veltman, Nucl. Phys. **B 50** (1972) 318.

[2] K. Hagiwara *et al.*, Nucl. Phys. **B 282** (1987) 253; G.J. Gounaris *et al.*, Phys. Rev. **D 61** (2000) 073013; J. Alcaraz *et al.*, Phys. Rev. **D 61** (2000) 075006.

[3] G.J. Gounaris *et al.*, Preprint hep-ph/0003143 (2000).

[4] S. Bar-Shalom *et al.*, Preprint hep-ph/0005295 (2000).

[5] K. Agashe and N.G. Deshpande, Phys. Lett. **B 456** (1999) 60; L3 Collab., M. Acciarri *et al.*, Phys. Lett. **B 464** (1999) 135; L3 Collab., M. Acciarri *et al.*, Phys. Lett. **B 470** (1999) 281; S. Mele and E. Sanchez, Phys. Rev. **D 61** (2000) 117901.

[6] L3 Collab., M. Acciarri *et al.*, Phys. Lett. **B 450** (1999) 281.

[7] L3 Collab., M. Acciarri *et al.*, Phys. Lett. **B 465** (1999) 363.

[8] OPAL Collab., G. Abbiendi *et al.*, Phys. Lett. **B 476** (2000) 256; ALEPH Collab., R. Barate *et al.*, Phys. Lett. **B 469** (1999) 287; DELPHI Collab., P. Abreu *et al.*, Preprint CERN-EP/2000-089 (2000).

[9] L3 Collab., B. Adeva *et al.*, Nucl. Inst. Meth. **A 289** (1990) 35; L3 Collab., O. Adriani *et al.*, Phys. Rep. **236** (1993) 1; I.C. Brock *et al.*, Nucl. Instr. Meth. **A 381** (1996) 236; M. Chemarin *et al.*, Nucl. Inst. Meth. **A 349** (1994) 345; M. Acciarri *et al.*, Nucl. Inst. Meth. **A 351** (1994) 300; A. Adam *et al.*, Nucl. Inst. Meth. **A 383** (1996) 342; G. Basti *et al.*, Nucl. Inst. Meth. **A 374** (1996) 293.

[10] R. Kleiss and R. Pittau, Comp. Phys. Comm. **85** (1995) 447; R. Pittau, Phys. Lett. **B 335** (1994) 490.

[11] PYTHIA version 5.722 is used, T. Sjöstrand, Preprint CERN–TH/7112/93 (1993), revised 1995; T. Sjöstrand, Comp. Phys. Comm. **82** (1994) 74.

[12] S. Jadach *et al.*, Comp. Phys. Comm **130** (2000) 206.

[13] KORALZ version 4.02 is used, S. Jadach *et al.*, Comp. Phys. Comm. **79** (1994) 503.

[14] S. Jadach *et al.*, Phys. Lett. **B 390** (1997) 298.

[15] KORALW version 1.21 is used, M. Skrzypek *et al.*, Comp. Phys. Comm. **94** (1996) 216; M. Skrzypek *et al.*, Phys. Lett. **B 372** (1996) 289.

[16] PHOJET version 1.05c is used, R. Engel, Z. Phys. **C 66** (1995) 203; R. Engel and J. Ranft, Phys. Rev. **D 54** (1996) 4244.

[17] F.A. Berends, P.H. Daverfelt and R. Kleiss, Nucl. Phys. **B 253** (1985) 441; Comp. Phys. Comm. **40** (1986) 285.

[18] GEANT version 3.15 is used, R. Brun *et al.*, Preprint CERN–DD/EE/84–1 (1984), revised 1987. The GHEISHA program (H. Fesefeldt, RWTH Aachen Report PITHA 85/02 (1985)) is used to simulate hadronic interactions.

[19] Particle Data Group, D.E. Groom *et al.*, Eur. Phys. J. **C 15** (2000) 1.

[20] J. Fujimoto *et al.*, Comp. Phys. Comm. **100** (1997) 128.

[21] S. Bethke *et al.*, Nucl. Phys. **B 370** (1992) 310.

[22] L3 Collab., M. Acciarri *et al.*, Phys. Lett. **B 479** (2000) 101.

[23] L3 Collab., M. Acciarri *et al.*, Preprint CERN-EP/2000-104 (2000).

[24] L3 Collab., M. Acciarri *et al.*, Phys. Lett. **B 431** (1998) 437; L3 Collab., M. Acciarri *et al.*, Phys. Lett. **B 436** (1998) 403; L3 Collab., M. Acciarri *et al.*, Phys. Lett. **B 461** (1999) 376.

[25] M.W. Grünewald *et al.*, Preprint hep-ph/0005309 (2000).

[26] S. Jadach *et al.*, Phys. Rev. **D56** (1997) 6939.

The L3 Collaboration:

M.Acciarri,[26] P.Achard,[19] O.Adriani,[16] M.Aguilar-Benitez,[25] J.Alcaraz,[25] G.Alemanni,[22] J.Allaby,[17] A.Aloisio,[28] M.G.Alviggi,[28] G.Ambrosi,[19] H.Anderhub,[48] V.P.Andreev,[6,36] T.Angelescu,[12] F.Anselmo,[9] A.Arefiev,[27] T.Azemoon,[3] T.Aziz,[10] P.Bagnaia,[35] A.Bajo,[25] L.Baksay,[43] A.Balandras,[4] S.V.Baldew,[2] S.Banerjee,[10] Sw.Banerjee,[10] A.Barczyk,[48,46] R.Barillère,[17] P.Bartalini,[22] M.Basile,[9] R.Battiston,[32] A.Bay,[22] F.Becattini,[16] U.Becker,[14] F.Behner,[48] L.Bellucci,[16] R.Berbeco,[3] J.Berdugo,[25] P.Berges,[14] B.Bertucci,[32] B.L.Betev,[48] S.Bhattacharya,[10] M.Biasini,[32] A.Biland,[48] J.J.Blaising,[4] S.C.Blyth,[33] G.J.Bobbink,[2] A.Böhm,[1] L.Boldizsar,[13] B.Borgia,[35] D.Bourilkov,[48] M.Bourquin,[19] S.Braccini,[19] J.G.Branson,[39] F.Brochu,[4] A.Buffini,[16] A.Buijs,[44] J.D.Burger,[14] W.J.Burger,[32] X.D.Cai,[14] M.Capell,[14] G.Cara Romeo,[9] G.Carlino,[28] A.M.Cartacci,[16] J.Casaus,[25] G.Castellini,[16] F.Cavallari,[35] N.Cavallo,[37] C.Cecchi,[32] M.Cerrada,[25] F.Cesaroni,[23] M.Chamizo,[19] Y.H.Chang,[50] U.K.Chaturvedi,[18] M.Chemarin,[24] A.Chen,[50] G.Chen,[7] G.M.Chen,[7] H.F.Chen,[20] H.S.Chen,[7] G.Chiefari,[28] L.Cifarelli,[38] F.Cindolo,[9] C.Civinini,[16] I.Clare,[14] R.Clare,[14] G.Coignet,[4] N.Colino,[25] F.Conventi,[28] S.Costantini,[5] F.Cotorobai,[12] B.de la Cruz,[25] A.Csilling,[13] S.Cucciarelli,[32] T.S.Dai,[14] J.A.van Dalen,[30] R.D'Alessandro,[16] R.de Asmundis,[28] P.Déglon,[19] A.Degré,[4] K.Deiters,[46] M.Della Pietra,[28] D.della Volpe,[28] E.Delmeire,[19] P.Denes,[34] F.DeNotaristefani,[35] A.De Salvo,[48] M.Diemoz,[35] M.Dierckxsens,[2] D.van Dierendonck,[2] C.Dionisi,[35] M.Dittmar,[48] A.Dominguez,[39] A.Doria,[28] M.T.Dova,[18,♯] D.Duchesneau,[4] D.Dufournaud,[4] P.Duinker,[2] I.Duran,[40] H.El Mamouni,[24] A.Engler,[33] F.J.Eppling,[14] F.C.Erné,[2] P.Extermann,[19] M.Fabre,[46] M.A.Falagan,[25] S.Falciano,[35,17] A.Favara,[17] J.Fay,[24] O.Fedin,[36] M.Felcini,[48] T.Ferguson,[33] H.Fesefeldt,[1] E.Fiandrini,[32] J.H.Field,[19] F.Filthaut,[17] P.H.Fisher,[14] I.Fisk,[39] G.Forconi,[14] K.Freudenreich,[48] C.Furetta,[26] Yu.Galaktionov,[27,14] S.N.Ganguli,[10] P.Garcia-Abia,[5] M.Gataullin,[31] S.S.Gau,[11] S.Gentile,[35,17] N.Gheordanescu,[12] S.Giagu,[35] Z.F.Gong,[20] G.Grenier,[24] O.Grimm,[48] M.W.Gruenewald,[8] M.Guida,[38] R.van Gulik,[2] V.K.Gupta,[34] A.Gurtu,[10] L.J.Gutay,[45] D.Haas,[5] A.Hasan,[29] D.Hatzifotiadou,[9] T.Hebbeker,[8] A.Hervé,[17] P.Hidas,[13] J.Hirschfelder,[33] H.Hofer,[48] G. Holzner,[48] H.Hoorani,[33] S.R.Hou,[50] Y.Hu,[30] I.Iashvili,[47] B.N.Jin,[7] L.W.Jones,[3] P.de Jong,[2] I.Josa-Mutuberría,[25] R.A.Khan,[18] M.Kaur,[18,◇] M.N.Kienzle-Focacci,[19] D.Kim,[35] J.K.Kim,[42] J.Kirkby,[17] D.Kiss,[13] W.Kittel,[30] A.Klimentov,[14,27] A.C.König,[30] M.Kopal,[45] A.Kopp,[47] V.Koutsenko,[14,27] M.Kräber,[48] R.W.Kraemer,[33] W.Krenz,[1] A.Krüger,[47] A.Kunin,[14,27] P.Ladron de Guevara,[25] I.Laktineh,[24] G.Landi,[16] M.Lebeau,[17] A.Lebedev,[14] P.Lebrun,[24] P.Lecomte,[48] P.Lecoq,[17] P.Le Coultre,[48] H.J.Lee,[8] J.M.Le Goff,[17] R.Leiste,[47] P.Levtchenko,[36] C.Li,[20] S.Likhoded,[47] C.H.Lin,[50] W.T.Lin,[50] F.L.Linde,[2] L.Lista,[28] Z.A.Liu,[7] W.Lohmann,[47] E.Longo,[35] Y.S.Lu,[7] K.Lübelsmeyer,[1] C.Luci,[17,35] D.Luckey,[14] L.Lugnier,[24] L.Luminari,[35] W.Lustermann,[48] W.G.Ma,[20] M.Maity,[10] L.Malgeri,[17] A.Malinin,[17] C.Maña,[25] D.Mangeol,[30] J.Mans,[34] G.Marian,[15] J.P.Martin,[24] F.Marzano,[35] K.Mazumdar,[10] R.R.McNeil,[6] S.Mele,[17] L.Merola,[28] M.Meschini,[16] W.J.Metzger,[30] M.von der Mey,[1] A.Mihul,[12] H.Milcent,[17] G.Mirabelli,[35] J.Mnich,[17] G.B.Mohanty,[10] T.Moulik,[10] G.S.Muanza,[24] A.J.M.Muijs,[2] B.Musicar,[39] M.Musy,[35] M.Napolitano,[28] F.Nessi-Tedaldi,[48] H.Newman,[31] T.Niessen,[1] A.Nisati,[35] H.Nowak,[47] R.Ofierzynski,[48] G.Organtini,[35] A.Oulianov,[27] C.Palomares,[25] D.Pandoulas,[1] S.Paoletti,[35,17] P.Paolucci,[28] R.Paramatti,[35] H.K.Park,[33] I.H.Park,[42] G.Passaleva,[17] S.Patricelli,[28] T.Paul,[11] M.Pauluzzi,[32] C.Paus,[17] F.Pauss,[48] M.Pedace,[35] S.Pensotti,[26] D.Perret-Gallix,[4] B.Petersen,[30] D.Piccolo,[28] F.Pierella,[9] M.Pieri,[16] P.A.Piroué,[34] E.Pistolesi,[26] V.Plyaskin,[27] M.Pohl,[19] V.Pojidaev,[27,16] H.Postema,[14] J.Pothier,[17] D.O.Prokofiev,[45] D.Prokofiev,[36] J.Quartieri,[38] G.Rahal-Callot,[48,17] M.A.Rahaman,[10] P.Raics,[15] N.Raja,[10] R.Ramelli,[48] P.G.Rancoita,[26] R.Ranieri,[16] A.Raspereza,[47] G.Raven,[39] P.Razis,[29] D.Ren,[48] M.Rescigno,[35] S.Reucroft,[11] S.Riemann,[47] K.Riles,[3] J.Rodin,[43] B.P.Roe,[3] L.Romero,[25] A.Rosca,[8] S.Rosier-Lees,[4] J.A.Rubio,[17] G.Ruggiero,[16] H.Rykaczewski,[48] S.Saremi,[6] S.Sarkar,[35] J.Salicio,[17] E.Sanchez,[17] M.P.Sanders,[30] M.E.Sarakinos,[21] C.Schäfer,[17] V.Schegelsky,[36] S.Schmidt-Kaerst,[1] D.Schmitz,[1] H.Schopper,[49] D.J.Schotanus,[30] G.Schwering,[1] C.Sciacca,[28] A.Seganti,[9] L.Servoli,[32] S.Shevchenko,[31] N.Shivarov,[41] V.Shoutko,[27] E.Shumilov,[27] A.Shvorob,[31] T.Siedenburg,[1] D.Son,[42] B.Smith,[33] P.Spillantini,[16] M.Steuer,[14] D.P.Stickland,[34] A.Stone,[6] B.Stoyanov,[41] A.Straessner,[1] K.Sudhakar,[10] G.Sultanov,[18] L.Z.Sun,[20] H.Suter,[48] J.D.Swain,[18] Z.Szillasi,[43,¶] T.Sztaricskai,[43,¶] X.W.Tang,[7] L.Tauscher,[5] L.Taylor,[11] B.Tellili,[24] C.Timmermans,[30] Samuel C.C.Ting,[14] S.M.Ting,[14] S.C.Tonwar,[10] J.Tóth,[13] C.Tully,[17] K.L.Tung,[7] Y.Uchida,[14] J.Ulbricht,[48] E.Valente,[35] G.Vesztergombi,[13] I.Vetlitsky,[27] D.Vicinanza,[38] G.Viertel,[48] S.Villa,[11] M.Vivargent,[4] S.Vlachos,[5] I.Vodopianov,[36] H.Vogel,[33] H.Vogt,[47] I.Vorobiev,[33] A.A.Vorobyov,[36] A.Vorvolakos,[29] M.Wadhwa,[5] W.Wallraff,[1] M.Wang,[14] X.L.Wang,[20] Z.M.Wang,[20] A.Weber,[1] M.Weber,[1] P.Wienemann,[1] H.Wilkens,[30] S.X.Wu,[14] S.Wynhoff,[17] L.Xia,[31] Z.Z.Xu,[20] J.Yamamoto,[3] B.Z.Yang,[20] C.G.Yang,[7] H.J.Yang,[7] M.Yang,[7] J.B.Ye,[20] S.C.Yeh,[51] An.Zalite,[36] Yu.Zalite,[36] Z.P.Zhang,[20] G.Y.Zhu,[7] R.Y.Zhu,[31] A.Zichichi,[9,17,18] G.Zilizi,[43,¶] B.Zimmermann,[48] M.Zöller.[1]

1 I. Physikalisches Institut, RWTH, D-52056 Aachen, FRG[§]
III. Physikalisches Institut, RWTH, D-52056 Aachen, FRG[§]
2 National Institute for High Energy Physics, NIKHEF, and University of Amsterdam, NL-1009 DB Amsterdam, The Netherlands
3 University of Michigan, Ann Arbor, MI 48109, USA
4 Laboratoire d'Annecy-le-Vieux de Physique des Particules, LAPP,IN2P3-CNRS, BP 110, F-74941 Annecy-le-Vieux CEDEX, France
5 Institute of Physics, University of Basel, CH-4056 Basel, Switzerland
6 Louisiana State University, Baton Rouge, LA 70803, USA
7 Institute of High Energy Physics, IHEP, 100039 Beijing, China[△]
8 Humboldt University, D-10099 Berlin, FRG[§]
9 University of Bologna and INFN-Sezione di Bologna, I-40126 Bologna, Italy
10 Tata Institute of Fundamental Research, Bombay 400 005, India
11 Northeastern University, Boston, MA 02115, USA
12 Institute of Atomic Physics and University of Bucharest, R-76900 Bucharest, Romania
13 Central Research Institute for Physics of the Hungarian Academy of Sciences, H-1525 Budapest 114, Hungary[‡]
14 Massachusetts Institute of Technology, Cambridge, MA 02139, USA
15 KLTE-ATOMKI, H-4010 Debrecen, Hungary[¶]
16 INFN Sezione di Firenze and University of Florence, I-50125 Florence, Italy
17 European Laboratory for Particle Physics, CERN, CH-1211 Geneva 23, Switzerland
18 World Laboratory, FBLJA Project, CH-1211 Geneva 23, Switzerland
19 University of Geneva, CH-1211 Geneva 4, Switzerland
20 Chinese University of Science and Technology, USTC, Hefei, Anhui 230 029, China[△]
21 SEFT, Research Institute for High Energy Physics, P.O. Box 9, SF-00014 Helsinki, Finland
22 University of Lausanne, CH-1015 Lausanne, Switzerland
23 INFN-Sezione di Lecce and Università Degli Studi di Lecce, I-73100 Lecce, Italy
24 Institut de Physique Nucléaire de Lyon, IN2P3-CNRS,Université Claude Bernard, F-69622 Villeurbanne, France
25 Centro de Investigaciones Energéticas, Medioambientales y Tecnologícas, CIEMAT, E-28040 Madrid, Spain[♭]
26 INFN-Sezione di Milano, I-20133 Milan, Italy
27 Institute of Theoretical and Experimental Physics, ITEP, Moscow, Russia
28 INFN-Sezione di Napoli and University of Naples, I-80125 Naples, Italy
29 Department of Natural Sciences, University of Cyprus, Nicosia, Cyprus
30 University of Nijmegen and NIKHEF, NL-6525 ED Nijmegen, The Netherlands
31 California Institute of Technology, Pasadena, CA 91125, USA
32 INFN-Sezione di Perugia and Università Degli Studi di Perugia, I-06100 Perugia, Italy
33 Carnegie Mellon University, Pittsburgh, PA 15213, USA
34 Princeton University, Princeton, NJ 08544, USA
35 INFN-Sezione di Roma and University of Rome, "La Sapienza", I-00185 Rome, Italy
36 Nuclear Physics Institute, St. Petersburg, Russia
37 INFN-Sezione di Napoli and University of Potenza, I-85100 Potenza, Italy
38 University and INFN, Salerno, I-84100 Salerno, Italy
39 University of California, San Diego, CA 92093, USA
40 Dept. de Fisica de Particulas Elementales, Univ. de Santiago, E-15706 Santiago de Compostela, Spain
41 Bulgarian Academy of Sciences, Central Lab. of Mechatronics and Instrumentation, BU-1113 Sofia, Bulgaria
42 Laboratory of High Energy Physics, Kyungpook National University, 702-701 Taegu, Republic of Korea
43 University of Alabama, Tuscaloosa, AL 35486, USA
44 Utrecht University and NIKHEF, NL-3584 CB Utrecht, The Netherlands
45 Purdue University, West Lafayette, IN 47907, USA
46 Paul Scherrer Institut, PSI, CH-5232 Villigen, Switzerland
47 DESY, D-15738 Zeuthen, FRG
48 Eidgenössische Technische Hochschule, ETH Zürich, CH-8093 Zürich, Switzerland
49 University of Hamburg, D-22761 Hamburg, FRG
50 National Central University, Chung-Li, Taiwan, China
51 Department of Physics, National Tsing Hua University, Taiwan, China
§ Supported by the German Bundesministerium für Bildung, Wissenschaft, Forschung und Technologie
‡ Supported by the Hungarian OTKA fund under contract numbers T019181, F023259 and T024011.
¶ Also supported by the Hungarian OTKA fund under contract numbers T22238 and T026178.
♭ Supported also by the Comisión Interministerial de Ciencia y Tecnología.
♯ Also supported by CONICET and Universidad Nacional de La Plata, CC 67, 1900 La Plata, Argentina.
◇ Also supported by Panjab University, Chandigarh-160014, India.
△ Supported by the National Natural Science Foundation of China.

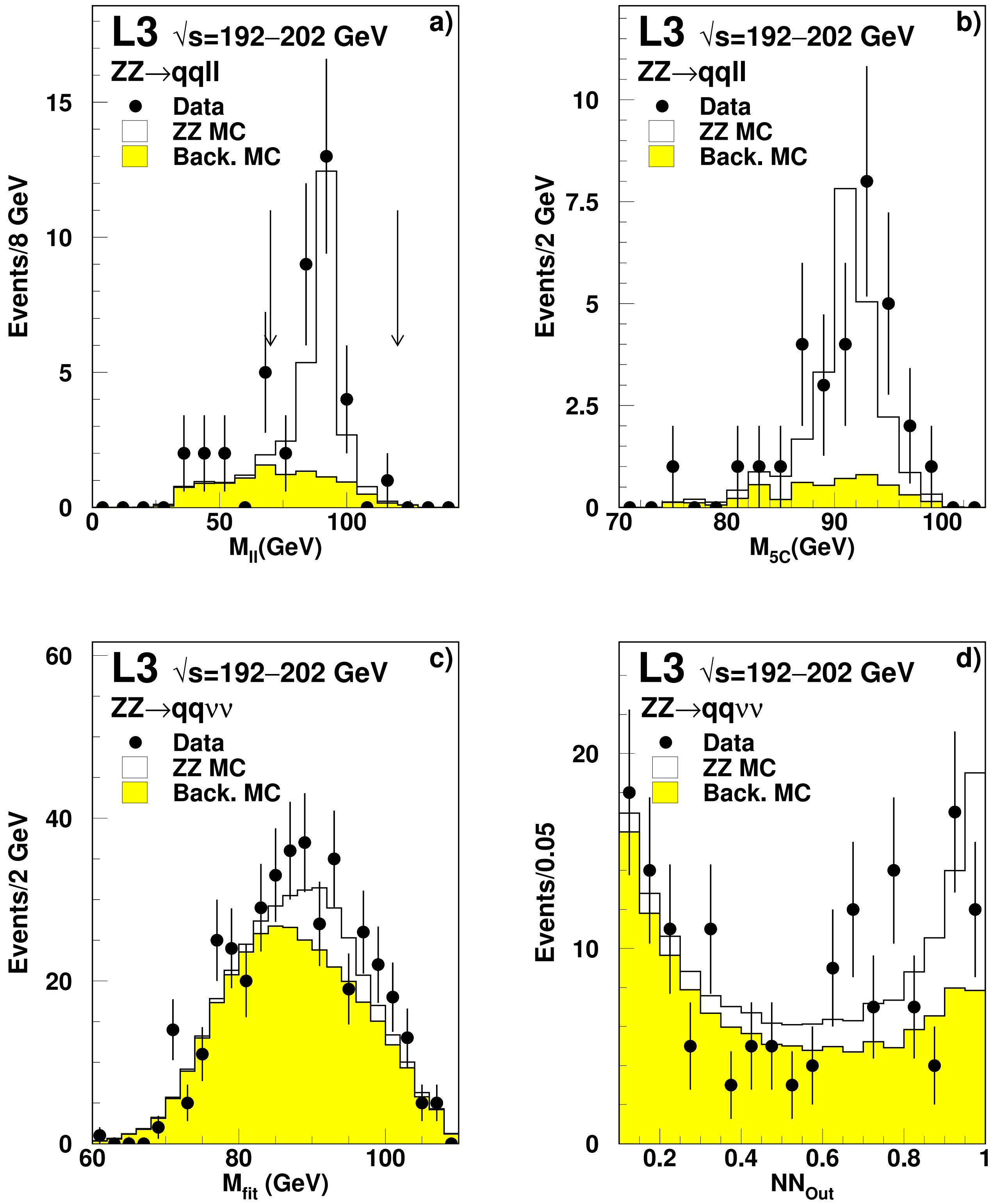

Figure 1: Distributions for data and Monte Carlo of: a) Invariant mass $M_{\ell\ell}$ of the lepton pair for the $\mathrm{q\bar{q}}\ell^+\ell^-$ final state before the application of the cuts indicated by the arrows. b) The fit mass M_{5C} of the $\mathrm{q\bar{q}}\ell^+\ell^-$ final state. c) The mass M_{fit} of the hadronic system of the $\mathrm{q\bar{q}}\nu\bar{\nu}$ final state after a kinematic fit that imposes the Z mass to the event missing four-momentum. d) The output NN_{Out} of the $\mathrm{q\bar{q}}\nu\bar{\nu}$ neural network. A cut at 0.1 is applied.

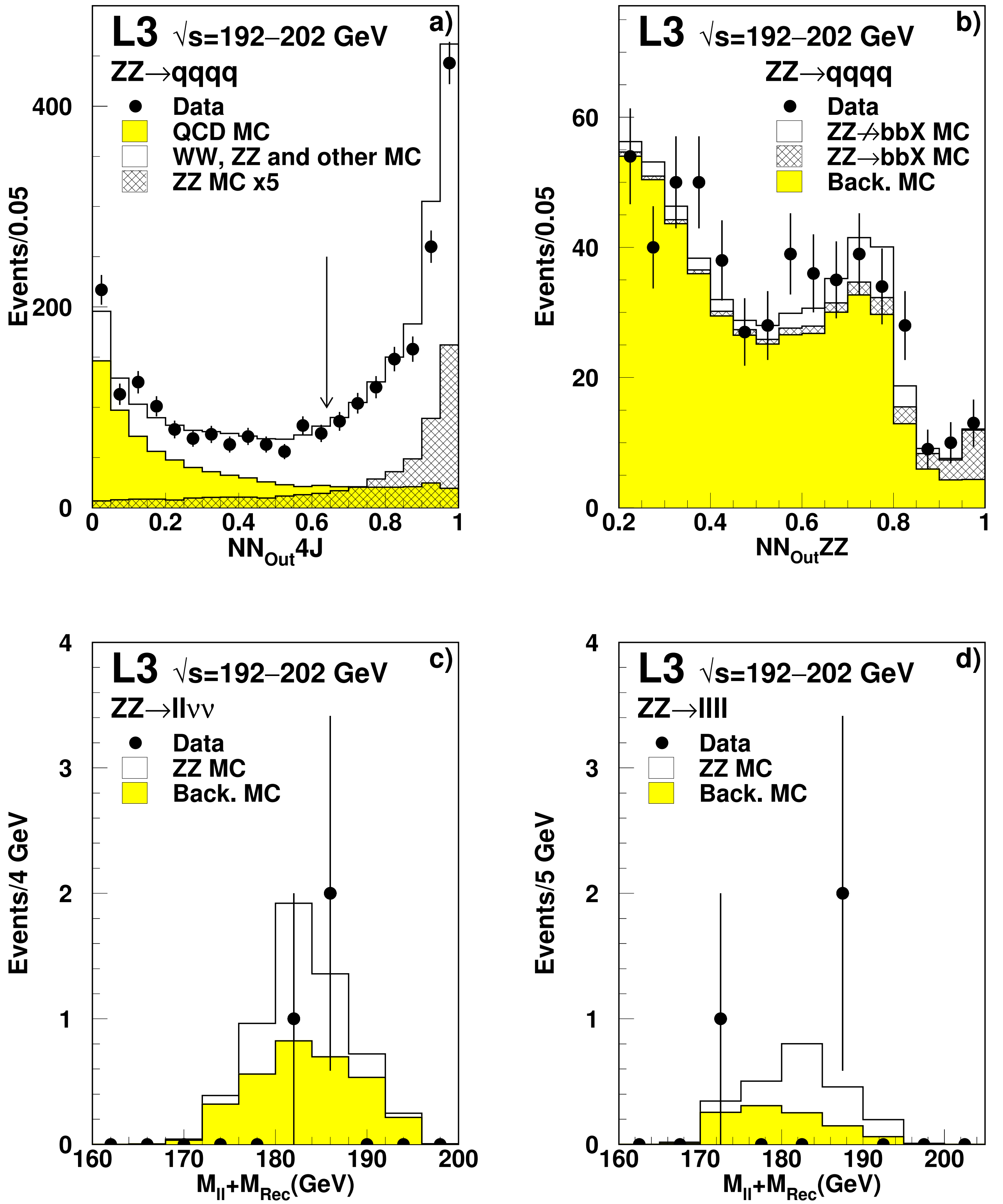

Figure 2: Distributions for the $q\bar{q}q'\bar{q}'$ selection of the outputs a) $NN_{Out}4J$ of the first neural network; the ZZ signal is superimposed with a cross section five times larger than the predicted one and the arrow shows the cut, b) $NN_{Out}ZZ$ of the final neural network; signal expectations for events with no or at least one b quark pair are presented separately. Distributions of the sum of the visible and recoil masses for c) the $\ell^+\ell^-\nu\bar{\nu}$ and d) the $\ell^+\ell^-\ell'^+\ell'^-$ selections. Data and Monte Carlo are shown.

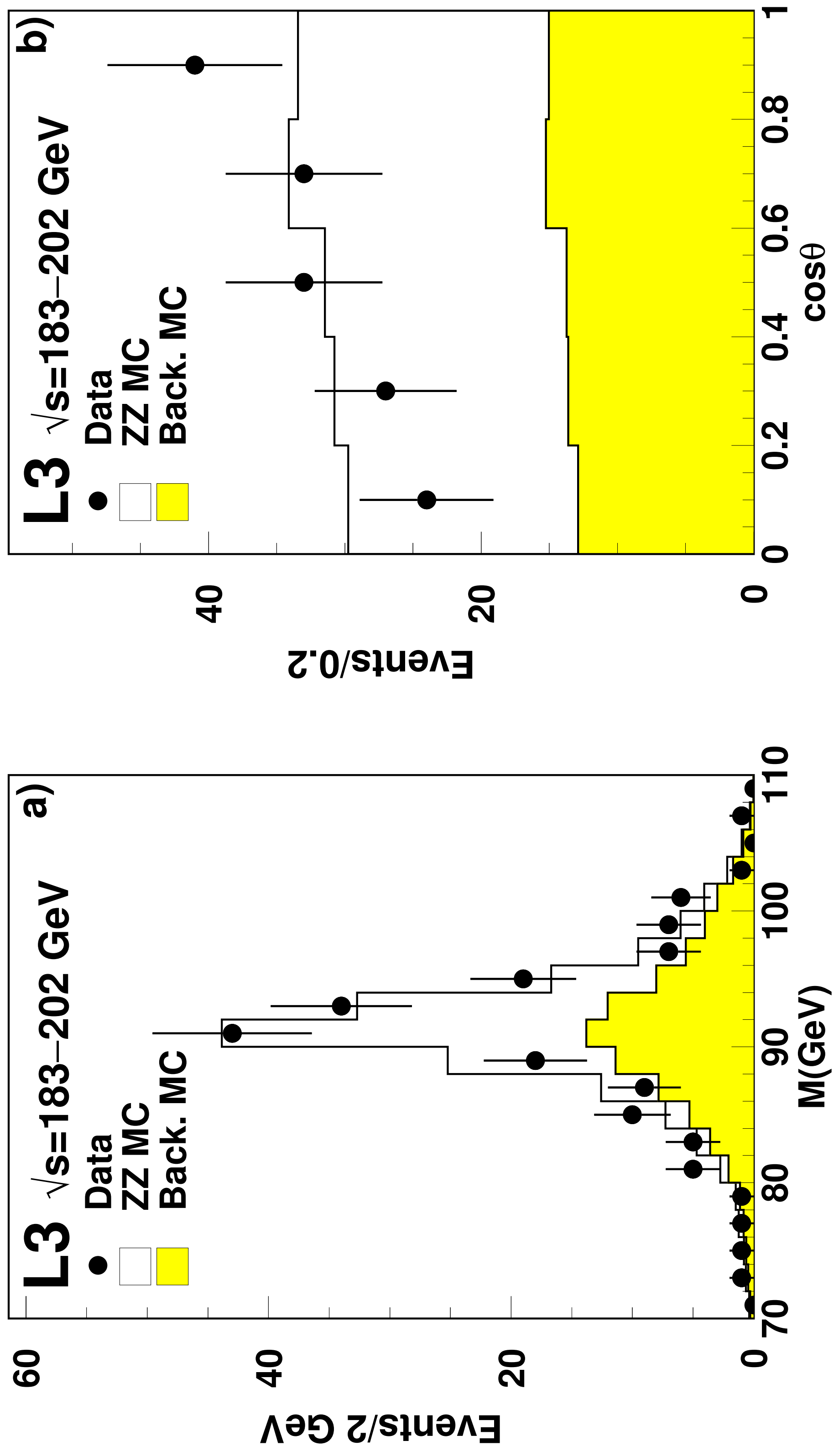

Figure 3: Distributions in data and Monte Carlo at all the LEP centre-of-mass energies above the Z pair production threshold of a) the reconstructed mass M and b) the cosine of the production angle θ. Cuts on the $\mathrm{q\bar{q}}\nu\bar{\nu}$ and $\mathrm{q\bar{q}q'\bar{q}'}$ neural network outputs are applied as 0.8 and 0.85, respectively.

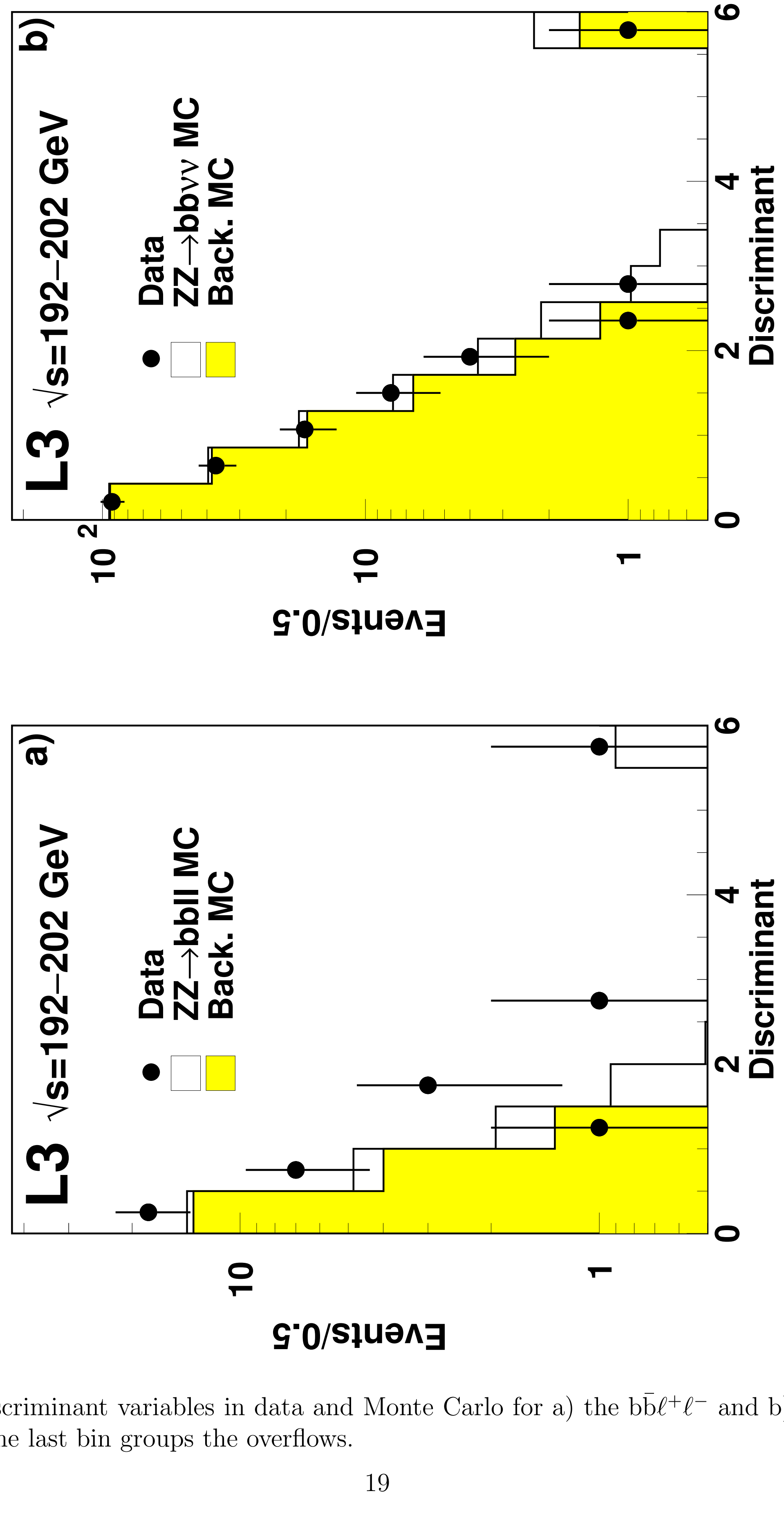

Figure 4: Discriminant variables in data and Monte Carlo for a) the $\mathrm{b\bar{b}}\ell^+\ell^-$ and b) the $\mathrm{b\bar{b}}\nu\bar{\nu}$ selections. The last bin groups the overflows.

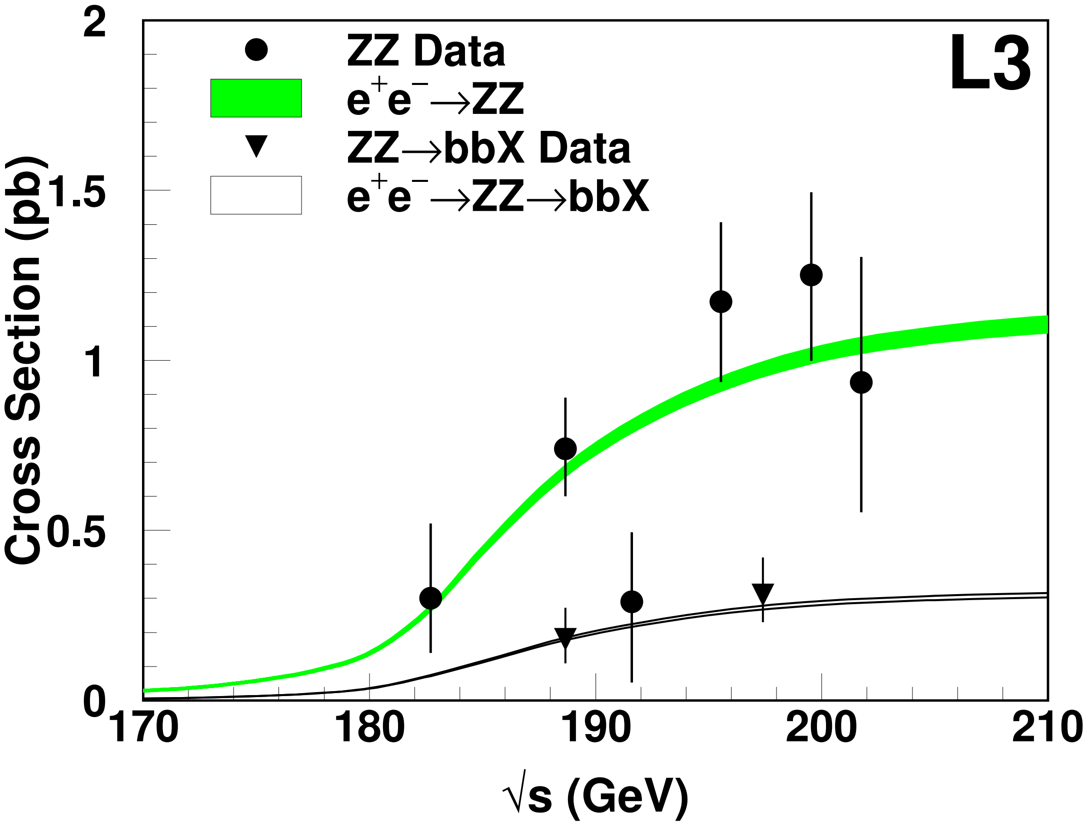

Figure 5: Measurements of the $e^+e^- \to$ZZ and ZZ $\to$ $b\bar{b}$X cross sections, where statistical and systematic uncertainties are combined in quadrature.